Acta Astronautica, Vol. 3, pp. 735–757. Pergamon Press 1976. Printed in the U.S.A.

Nonlinear behavior of acoustic waves in combustion chambers—II

F. E. C. CULICK
California Institute of Technology, Pasadena, CA 91109, U.S.A.

(*Received* 15 *September* 1975; *revised* 4 *March* 1976)

Abstract—The approximate analysis developed in Part I of this work is applied to several specific problems. One purpose is to illustrate the use of the formalism, and a second is to demonstrate the validity of the method by comparing results with numerical solutions, obtained elsewhere, for the "exact" equations. A simple problem is treated first, the decay of a standing wave in a box containing a mixture of gas and suspended particles; one example of the steepening of an initially sinusoidal wave in pure gas is included. Viscous losses on an inert surface are treated essentially according to classical linear theory; recent experimental results are used as the basis for incorporating approximately the influence of nonlinear heat transfer in unsteady flow. All of the preceding results are combined in calculations of two examples of unstable motions in a solid propellant rocket motor and in a *T*-burner.

1. Introduction

In the first part of this work (Culick, 1976), hereafter referred to as I, a general formalism is described for treating both linear and nonlinear processes associated with acoustic waves in combustion chambers. The method is suitable for studying many problems involving waves in chambers; a few relatively simple examples are described here. Ultimately, specific results can be obtained only by numerical integration of a set of coupled nonlinear first-order ordinary differential equations. One of the purposes of this paper is to show how the representations of certain kinds of physical processes are incorporated prior to numerical computations. For convenience in reading, a brief summary of the development of the analysis is given below. Some of the formulas required in subsequent discussion are included, but Part I will frequently be referred to in later sections.

It is simplest to treat problems involving no flow or combustion. The analysis then describes the development of waves in a closed chamber. Some examples for the attenuation of waves in a gas containing particles are given in Section 2; a special case is the steepening of sinusoidal waves into triangular waves in a pure gas containing no particles. Some comparisons are made with "exact" numerical solutions to the conservation equations for one-dimensional motions. For the conditions examined, the approximate analysis appears to be quite accurate, and is, of course, considerably cheaper to use.

The viscous losses at inert surfaces are often important; these are treated in Section 3. For linear behavior, the classical results are derived in a slightly different manner from that usually given. Some recent global measurements of losses are incorporated to provide a means of estimating the effect of nonlinear behavior.

Preliminary to treating unstable waves in combustion chambers, an approximate way of accounting for transient combustion is discussed in Section 4. Finally, in Section 5 unstable motions in a small solid propellant rocket motor and in a T-burner are analyzed. The discussion is intended only to provide illustrations of the method, and not as an exhaustive account. Once again, comparisons with numerical solutions are made.

All of the examples discussed here involve only longitudinal modes, for which the natural frequencies are integral multiples of the fundamental. Formulas valid for any geometry, i.e. any set of normal modes, have been deduced by Culick (1975), but to date no numerical results have been obtained. Eventually, an important application of the approximate analysis will be for three-dimensional problems which are prohibitively expensive to solve by more exact numerical techniques. It is a necessary preliminary step to demonstrate the validity of the approximate analysis, as far as possible, by the sorts of comparisons with "exact" solutions discussed here.

In broad outline, the formalism of the approximate analysis is developed in the following three steps. The conservation equations are first manipulated (Section 2 of I) to produce a nonlinear inhomogeneous wave equation for the pressure disturbances, with an inhomogeneous boundary condition:

$$\frac{1}{\bar{a}^2}\frac{\partial^2 p'}{\partial t^2} - \nabla^2 p' = -h \tag{1.1}$$

$$\hat{n} \cdot \nabla p' = -f. \tag{1.2}$$

The functions h and f contain representations of all perturbations of the classical acoustics problem for the actual geometry being considered. Two important points should be noted. First, the speed of sound $\bar{a}$, and other physical properties not explicitly shown, are those for a two-phase (or in general a multiphase) mixture. This is a consequence of combining the original conservation equations to give a description of the flow as that for a single average fluid. Second, the forms of the functions h and f depend on what order of perturbations are considered. The procedure is based on expansion in two small parameters, the Mach numbers $\bar{M}$ and M' of the average and fluctuating flows. Terms in h and f which are linear in M' also depend linearly on $\bar{M}$; these produce results for problems of stability. In the present work, nonlinear terms from the gasdynamics are carried to order M'^2 only and are independent of $\bar{M}$. Other nonlinear terms will arise, for example, in the treatment of nonlinear particle damping discussed in Section 2.

The second step is based on expansion of the unsteady pressure and velocity fields in normal modes $\psi_i(\mathbf{r})$ of the chamber, with time-varying amplitudes $\eta_i(t)$:

$$\frac{p'}{p_o} = \sum_{i=0}^{\infty} \eta_i(t)\psi_i(\mathbf{r}) \tag{1.3}$$

$$\mathbf{u}' = \sum_{i=1}^{\infty} \frac{\dot{\eta}_i(t)}{\bar{\gamma}k_i^2}\nabla\psi_i(\mathbf{r}) \tag{1.4}$$

where $k_i = \bar{a}\omega_i$ is the wavenumber for the ith mode. After (1.1) has been multiplied by $\psi_n(\mathbf{r})$ and integrated over the volume of the chamber, the ordinary differential equation for $\eta_n(t)$ can be deduced:

$$\frac{d^2\eta_n}{dt^2} + \omega_n^2\eta_n = F_n \tag{1.5}$$

with

$$F_n = -\frac{\bar{a}^2}{p_0 E_n^2}\left\{\int\int\int \psi_n h \, dV + \oint\oint \psi_n f \, dS\right\}. \tag{1.6}$$

Finally, in the third step, the method of averaging is applied to reduce the second order equations (1.5) to first order equations. The amplitudes are written

$$\eta_n = A_n(t)\sin\omega_n t + B_n(t)\cos\omega_n t, \tag{1.7}$$

and averaging over the time interval $(t, t+\tau)$ leads to the first order equations for the $A_n(t)$ and the $B_n(t)$:

$$\frac{dA_n}{dt} = \frac{1}{\omega_n\tau}\int_t^{t+\tau} F_n \cos\omega_n t' \, dt', \tag{1.8}$$

$$\frac{dB_n}{dt} = \frac{-1}{\omega_n\tau}\int_t^{t+\tau} F_n \sin\omega_n t' \, dt'. \tag{1.9}$$

For the special case of longitudinal modes ($\omega_n = n\omega_1$), the interval of averaging is taken as the period of the fundamental mode, $\tau = \tau_1 = 2\pi/\omega_1$, and the limits on the integrals may be changed to $(0, \tau_1)$ for any function F_n arising in problems of interest in this work.

If only the nonlinearities arising from the gasdynamics are shown, the force F_n has the general form

$$F_n = -\sum_{i=1}^{\infty}[D_{ni}\dot{\eta}_i + E_{ni}\eta_i] - \sum_{i=1}^{\infty}\sum_{j=1}^{\infty}[A_{nij}\dot{\eta}_i\dot{\eta}_j + B_{nij}\eta_i\eta_j]. \tag{1.10}$$

For longitudinal modes, F_n simplifies considerably (see Part I) and the equations (1.8) and (1.9) are

$$\frac{dA_n}{dt} = \alpha_n A_n + \theta_n B_n + \frac{\beta n}{2}\sum_{i=1}^{\infty}[A_i(A_{n-i} - A_{i-n} - A_{n+i}) - B_i(B_{n-i} + B_{i-n} + B_{n+i})] \tag{1.11}$$

$$\frac{dB_n}{dt} = \alpha_n B_n - \theta_n A_n + \frac{\beta n}{2}\sum_{i=1}^{\infty}[A_i(B_{n-i} + B_{i-n} - B_{n+i}) + B_i(A_{n-i} - A_{i-n} + A_{n+i})]. \tag{1.12}$$

The linear coefficients α_n, θ_n are related to the coefficients D_{nn}, E_{nn} in (1.10) by

$$\alpha_n = \frac{1}{2} D_{nn}, \quad \theta_n = \frac{1}{2\omega_n} E_{nn}. \tag{1.13}$$

This is a useful rule, because α_n is the familiar growth constant for linear motions, and θ_n is proportional to the shift of frequency.

2. An approximation to the linear and nonlinear attenuation of waves by gas/particle interactions

Particularly in solid propellant rockets using metallized propellants, but in other systems as well, some of the combustion products appear in the form of liquid or solid particles. The viscous interactions between the particles and the gas may, under suitable conditions, provide a significant dissipation of energy. It is often the case that the Reynolds number based on the particle diameter is outside the range in which Stokes' law is valid; it is necessary to use a more realistic representation of the drag force. This introduces another nonlinear influence in the general problem.

Let $F_n^{(p)}$ denote that part of F_n in eqn (1.6), representing the influences of inert particles. The terms involved are those containing $\delta \mathbf{F}_p'$ and $\delta Q_p'$, the fluctuations of (2.8) and (2.9) in I. By tracing the development in I from (2.10) and (2.11) to (3.16), with H defined by (3.15) in I, one finds that the terms in question are

$$F_n^{(p)} = \frac{\bar{\gamma}}{\rho_0 E_n^2} \int \frac{1}{\epsilon} \left[\frac{1}{\bar{a}^2} \frac{\bar{R}}{\bar{C}_v} \frac{\partial}{\partial t} (\delta Q_p' + \delta \mathbf{u}_p' \cdot \mathbf{F}_p) \psi_n + \delta \mathbf{F}_p' \cdot \nabla \psi_n \right] \mathrm{d}V. \tag{2.1}$$

Formulas for $\delta F_p'$ and $\delta Q_p'$ can be found only by solving the equations of motion for the particles. Numerical calculations (Levine and Culick, 1972; 1974) have shown that for many practical cases, nonlinear interactions are likely to be important. The approximate analysis here will be based on the nonlinear laws for the force $\mathbf{F}_p$ and heat transfer Q_p used in those works:

$$\mathbf{F}_p = \bar{\rho}_p \frac{18\mu}{\rho_s \sigma^2} (\mathbf{u}_p - \mathbf{u}) \left[1 + \frac{1}{6} Re^{2/3} \right] \tag{2.2}$$

$$Q_p = \bar{\rho}_p \frac{12 C_v \mu}{Pr \rho_s \sigma^2} (T_p - T)[1 + 0.23 Pr^{0.33} Re^{0.55}] \tag{2.3}$$

where

$$Re = \frac{\rho_{00} \sigma}{\mu} |\mathbf{u}_p - \mathbf{u}|. \tag{2.4}$$

Hereafter, the real flow will be treated only in a local approximation so that the particle motions may be treated as one-dimensional; interactions between particles are assumed to be negligible. Results will be given for steady-state harmonic motion; short term transient motions are neglected. Details of the analysis may be found in the report by Culick (1975). The linear part of the force,

for longitudinal modes, is

$$[F_n^{(\varphi)}]_{\text{lin}} = -\frac{\kappa}{1+\kappa}\left[X_1 + (\bar{\gamma}-1)\frac{C}{\bar{C}_p}X_2\right]\dot{\eta}_n - \omega_n\frac{\kappa}{1+\kappa}\left[\frac{\Omega_d^2}{1+\Omega_d^2} + (\bar{\gamma}-1)\frac{C}{\bar{C}_p}\frac{\Omega_t^2}{1+\Omega_t^2}\right] \tag{2.5}$$

where

$$X_1 = (\omega_n\Omega_d)/(1+\Omega_d^2) \tag{2.6}$$

$$X_2 = (\omega_n\Omega_t)/(1+\Omega_t^2). \tag{2.7}$$

A point not to be forgotten when this result is used is that the entire approximate analysis is founded on an iteration/perturbation procedure. This strictly requires that the force F_n on the right hand side of the oscillator equation $\ddot{\eta}_n + \omega_n^2\eta_n = F_n$ be small, in the sense of the inequality

$$F_n \ll \omega_n^2\eta_n.$$

Application of this constraint to the first term of (2.25) gives the requirement

$$\frac{\kappa}{1+\kappa}\frac{\Omega_d}{1+\Omega_d^2} \ll 1. \tag{2.8}$$

Because the procedure followed here is different from that used by Temkin and Dobbins (1966) to treat this problem, so also are the limits of validity. Their simplified results, which exhibit the same frequency dependence as (2.20) and (2.21), are valid for $\kappa \ll 1$. Consequently, the present formulation should have the advantage of being applicable over a broader range of particle loading.

By applying the rule (1.13) above, one finds for the linear contributions from gas/particle interactions:

$$\alpha_n^{(\varphi)} = -\frac{1}{2}\left(\frac{\kappa}{1+\kappa}\right)\left[X_1 + (\bar{\gamma}-1)\frac{C}{\bar{C}_p}X_2\right] \tag{2.9}$$

$$\theta_n^{(\varphi)} = \frac{\omega_n}{2}\left(\frac{\kappa}{1+\kappa}\right)\left[\frac{\Omega_d^2}{1+\Omega_d^2} + (\bar{\gamma}-1)\frac{C}{\bar{C}_p}\frac{\Omega_t^2}{1+\Omega_t^2}\right]. \tag{2.10}$$

Recent numerical results reported by Levine and Culick (1974) have shown that the result (2.9) is quite good for smaller particles, and if the frequency is not too high. Beyond limits which are presently not well-defined, the Reynolds number (2.4) becomes too large for the linear drag and heat transfer laws to be accurate. Further comments on the accuracy and some examples are given below.

The problem of analyzing nonlinear particle motions is avoided here. A correct treatment would involve solving the equations of motion with the nonlinear laws (2.2) and (2.3). A very much simpler course is taken here: the linear solutions are used to compute the next approximation in an iteration procedure (Culick, 1975).

Eventually the terms to be incorporated in the equations for the A_n and B_n are found to be:

$$\left[\frac{dA_n}{dt}\right]^{(p)}_{nonlin} = \omega_n\left(\frac{\kappa}{1+\kappa}\right)\{V_{n1}(B_n - \Omega_d A_n) + V_{n2}(B_n - \Omega_t A_N)\} \tag{2.11}$$

$$\left[\frac{dB_n}{dt}\right]^{(p)}_{nonlin} = \omega_n\left(\frac{\kappa}{1+\kappa}\right)\{V_{n1}(-A_n - \Omega_d B_n) + V_{n2}(-A_n - \Omega_t B_n)\} \tag{2.12}$$

where

$$V_{n1} = \frac{1.396}{\pi} W_{n1}(A_n^2 + B_n^2)^{0.331}, \tag{2.13}$$

$$V_{n2} = \frac{0.918}{\pi} W_{n2}(A_n^2 + B_n^2)^{0.275}. \tag{2.14}$$

$$W_{n1} = \frac{2}{\pi}(0.698)(1+\Omega_d^2)^{\xi_1/2} K_1\left(\frac{\bar{a}X_1}{\bar{\gamma}\omega_n}\right)^{\xi_1}\left(\frac{X_1}{\omega_n\Omega_d}\right), \tag{2.15}$$

$$W_{n2} = \frac{2}{\pi}(0.644)(1+\Omega_d^2)^{\xi_2/2}(\bar{\gamma}-1)\frac{C}{\bar{C}_p} K_2\left(\frac{\bar{a}X_1}{\bar{\gamma}\omega_n}\right)^{\xi_2}\left(\frac{X_2}{\omega_n\Omega_t}\right). \tag{2.16}$$

A few results have been obtained for the attenuation of a standing wave initially excited in a box of length L containing a gas/particle mixture. These have been carried out for direct comparison with the numerical results reported by Levine and Culick (1974). First, one case will be given in some detail. The particle diameter is 2.5μ, the particle loading is $\kappa = 0.36$ and the frequency based on the equilibrium speed of sound $\bar{a}$ is 800 Hz in each .se. The material and thermodynamic properties are listed below:

Specific heat of the gas	$C_p = 2021.8$ J/kgm-°K
Specific heat of the particle material	$C_s = 0.68C_p$
Isentropic exponent of the gas	$\gamma = 1.23$
Prandtl number	$Pr = 0.8$
Temperature	$T = 3416$°K
Pressure	$P_0 = 500$ psi
Viscosity of the gas	$\mu = 8.834 \times 10^{-4}\left(\frac{T}{3485}\right)^{0.66}$ kgm/m-sec
Density of the condensed material	$\rho_s = 1766$ kgm/m^3
The initial amplitude of the disturbance is	$\Delta p/p_0 = 0.15$.

Figures 2.1 and 2.2 show the waveforms obtained from the approximate and numerical analyses. The approximate results are the solutions to eqns (1.11) and (1.12) with the linear coefficients α_n, θ_n given by (2.9) and (2.10) and with additional nonlinear terms by (2.11) and (2.12). The period used to normalize the time scale is the period $2L/\bar{a}$ for linear waves based on the speed of sound of the

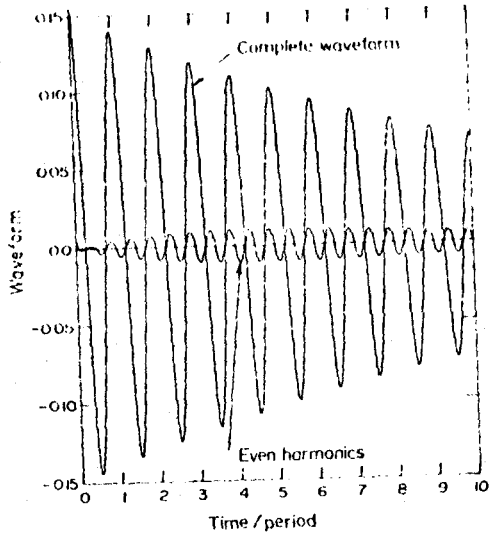

Fig. 2.1. Attenuation by 2.5-μ particles at 800 Hz according to the approximate analysis. $\Delta p(0)/p_o = 0.15$.

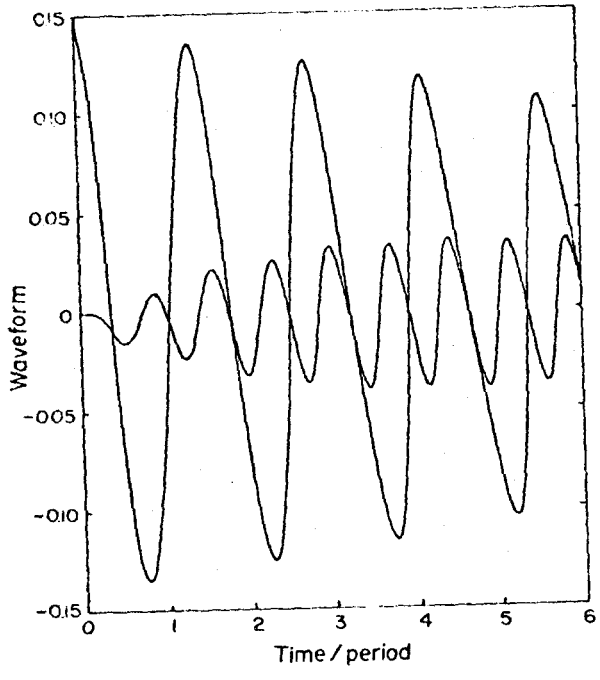

Fig. 2.2. Attenuation by 2.5-μ particles at 800 Hz according to the numerical analysis. $\Delta p(0)/p_o = 0.15$.

mixture. The similarities between the waveforms and the generation and decay of the even harmonics is apparent, but there is a difference in the relative phases between the even harmonics and the total waveform. This seems to arise almost entirely in the first cycle of the oscillation; it may be due to details of the numerical routines and the way in which the computations begin. This difference may therefore not reflect a genuine difference between the approximate and "exact" analyses.

A more quantitative measure of the behavior is the instantaneous value of the decay constant, α_p, calculated for successive peaks of the waveform. This history of α_p is shown in Fig. 2.3. Further remarks on the behavior of α_p may be found in

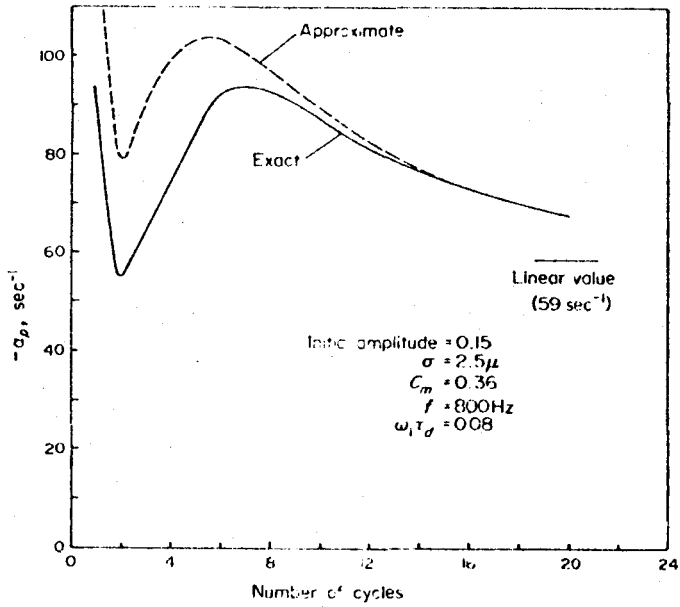

Fig. 2.3. The decay constant for the cases shown in Figs. 2.1 and 2.2.

Section 7 of the report by Levine and Culick (1974). The purpose here is only to demonstrate that the approximate analysis does give fairly reasonable results for this case. However, there are limitations, not yet clearly defined, which arise from the approximate treatment of the nonlinear acoustics as well as the gas/particle interactions.

The linear behavior used here, described essentially by velocity and temperature lags, is in fact quite restrictive. Although it is not apparent from the analyses presented here, the work reported by Levine and Culick shows that the results are accurate only when $\omega\tau_d$ is small. If this condition is met, then δu_p and δT_p are relatively small, which is consistent with the general nature of the perturbation analysis used here. For the 2.5-μ particles, $\omega\tau_d \approx 0.08$ at 800 Hz.

A case exhibiting more nonlinear behavior is shown in Fig. 2.4. The waveform calculated with the approximate analysis is shown for 30-μ particles at 1500 Hz

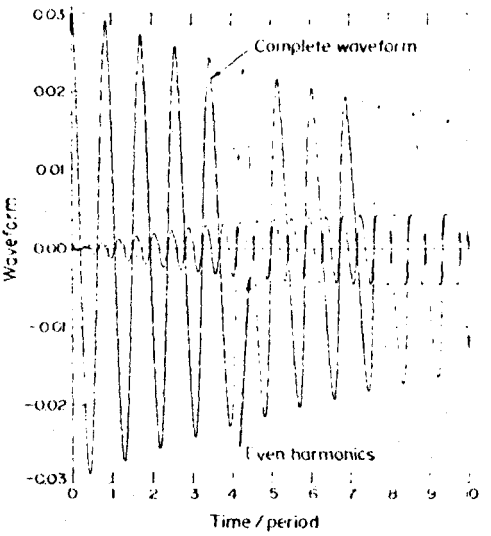

Fig. 2.4. Attenuation by 30-μ particles at 1500 Hz according to the approximate analysis; $\Delta p(0)/p_o = 0.03$.

($\omega\tau_d \approx 25.8$). The value of α_p is -70 sec^{-1} at an amplitude of 1%, and the numerical analysis gives -148 sec^{-1}. Note that the fractional error between the approximate and numerical results for α_p increases with increasing $\omega\tau_d$. The greater amount of harmonic content present when larger particles are considered is due mostly to the reduced drag and hence reduced attenuation at the higher frequencies. The results from the approximate analysis can be improved for higher values of $\omega\tau_d$ by using different functions X_1, X_2 instead of (2.6) and (2.7).

Wave propagation in a gas/particle mixture is dispersive; the speed of propagation depends on the frequency and particle size, through the parameter $\omega\tau_d$, as well as on the amount of condensed material present. For the problems treated here, the length of the box, and hence the wavelength of the waves, is fixed. Consequently, a change in the speed of sound is reflected as a shift of frequency. The periods of the waveforms shown in Figs. 2.1, 2.2 and 2.4 are not exactly equal to the period based on the equilibrium speed of sound. It is obvious from the figures that the frequency shift increases with $\omega\tau_d$. In Section 5 of Part I, it is shown that to first order, the frequency shift due to linear dispersion is $\delta f = -\theta/2\pi$; here, θ is given by (2.10) for the nth mode. The actual frequency change is dominated by θ_1; values of θ_1 and δf calculated from the waveforms for several cases are given in Table 2.1, a summary of the computations discussed here.

These results serve to demonstrate that the nonlinear generation of harmonics has substantial influence of the detailed character of the attenuation of waves. The rather close agreement between the approximate results and the numerical calculations under conditions when the approximation to the gas/particle interaction is more accurate suggests that the approximate treatment of the fluid mechanics is realistic, at least for moderate amplitudes.

Table 2.1. Summary of results for waves attenuated in a gas/particle mixture

Particle Diameter (μ)	f_e (Hz)	f_f (Hz)	f	$\omega\tau_d$	δf (Hz)	θ_1 2π	$(\alpha_p)_{lin}$ (sec^{-1})	$(\alpha_p)_{calc}$ (sec^{-1})
2.5								
Approximate	800	954	800	0.08	1	0.74	−59	−61
Numerical	800	954	801	0.08	1	—	−58	−59
Approximate	1500	1788	1505	0.15	5	4.8	−203	−204
Numerical	1500	1788	1504	0.15	4	—	−201	−204
10								
Approximate	1500	1788	1695	2.4	195	189.9	−509	−530
Numerical	1500	1788	1740	2.8	240	—	−509	−870
30								
Approximate	1500	1788	1740	21.6	240	224.1	−67	−70
Numerical	1500	1788	1787	25.8	287	—	−69	−148

f_e frequency based on the equilibrium

f_f frequency based on the speed for the gas only, $a_e = [(\gamma - 1)C_pT]^{1/2}$

f frequency of the calculated wave

$\delta f = f - f_e$

$(\alpha_p)_{lin}$ decay constant for linear waves

$(\alpha_p)_{calc}$ decay constant for the calculated wave at approximately 1% amplitude

Note. Small differences arise in some quantities ($\omega\tau_d$ and $(\alpha_p)_{lin}$) which should have the same values when calculated by the approximate and numerical methods. This is due to a small difference in the value of some property, most probably the viscosity.

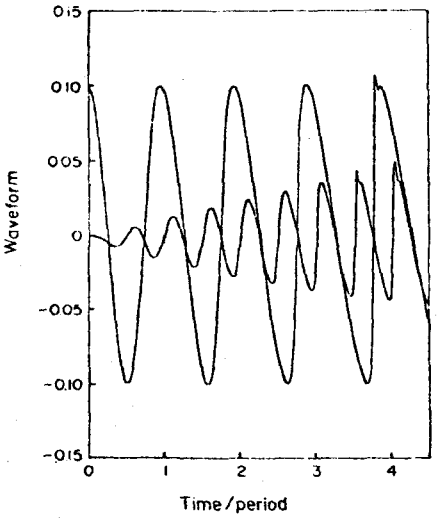

Fig. 2.5. Steepening of a standing wave in a pure gas according to the numerical analysis; $f = 900$ Hz.

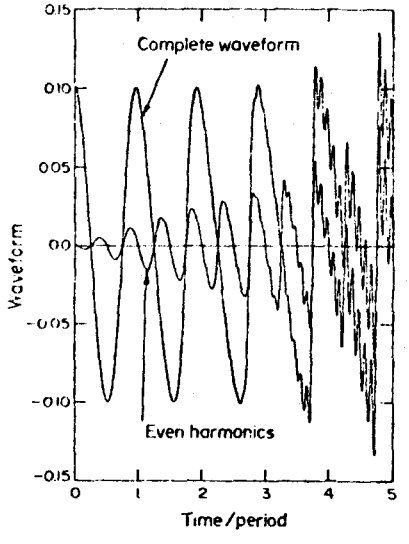

Fig. 2.6. Steepening of a standing wave in a pure gas according to the approximate analysis with ten modes accounted for; $f = 900$ Hz.

From the point of view of reducing data for the attenuation by particle/gas interactions, it is annoying that the value of the decay constant changes so much as the waves die out (cf. Fig. 2.3). It is possible that if the higher harmonics are filtered from the waveform, the behavior of α for the first harmonic alone may not be so extreme. Calculations have not been done to check this point.

Perhaps the simplest check of the fluid mechanics alone is calculation of the behavior of a wave in a box with no particles present. In this case, the wave must of course steepen, eventually forming a shock wave. Neither the exact nor approximate analyses can accommodate strong shock waves, but the initial period of development may usefully be examined. Figure 2.5 shows the exact result, and Fig. 2.6 shows the result of the approximate analysis when ten modes are accounted for. Again, the qualitative agreement is quite good. As one would anticipate, the period of the wave decreases as the amplitude increases. For both the approximate and numerical analyses, obvious distortion of the peak occurs at about the fourth cycle. (The sharp jags in Fig. 2.5 may be due in part of the numerical routine.)

3. An approximation to nonlinear viscous losses on an inert surface

There are two reasons for examining the influence of viscous stresses and heat transfer at an inert surface: these processes can be significant stabilizing influences; and in the presence of oscillations, the average heat transfer increases substantially. The second is a nonlinear effect which has on occasion caused serious structural problems, particularly in liquid rocket motors. The main purpose of this section is to show one way of incorporating some experimental results within the analysis developed earlier. As part of the argument, the more familiar linear results will also be recovered.

The viscous stresses and heat transfer at a surface are, of course, associated with a boundary layer, but they can be accommodated here by suitable interpretation of the force F and heat source Q in the equations developed in Part I. It is only those terms which are required in this discussion, so the wave equation for the pressure fluctuation is simply

$$\frac{\partial^2 p'}{\partial t^2} - \bar{a}^2 \nabla^2 p' = \frac{\bar{R}}{\bar{C}_v} \frac{\partial Q'}{\partial t} - \bar{a}^2 \nabla \cdot \mathbf{F}'. \tag{3.1}$$

The boundary condition is

$$\hat{n} \cdot \nabla p' = \hat{n} \cdot \mathbf{F}'. \tag{3.2}$$

For this problem, then, the equation for the amplitude of the nth harmonic is

$$\ddot{\eta}_n + \omega_n^2 \eta_n = \frac{\bar{\gamma}}{\rho_0 \bar{a}^2 E_n^2} \left\{ \frac{\bar{R}}{\bar{C}_v} \frac{\mathrm{d}}{\mathrm{d}t} \int Q' \psi_n \, \mathrm{d}V - \bar{a}^2 \int \mathbf{F}' \cdot \nabla \psi_n \, \mathrm{d}V \right\}. \tag{3.3}$$

The heat source Q' is taken here to be associated with the heat flux vector $\bar{q}'$, and

the force **F** with the viscous stress tensor $\bar{\tau}$:

$$Q' = \nabla \cdot \mathbf{q}' \quad \mathbf{F}' = \nabla \cdot \bar{\tau}'. \tag{3.4}$$

Both $\mathbf{q}'$ and $\bar{\tau}'$ are significantly non-zero only in thin regions near the boundary. Then if y denotes the coordinate normal to the wall, measured positive inward, $d = \mathrm{d}y\,\mathrm{d}S$ and

$$Q' = \frac{\partial q_y'}{\partial y} \quad \mathbf{F}' = \frac{\partial \tau_y'}{\partial y}. \tag{3.5}$$

The conventions used here are that q_y', the component of $\mathbf{q}'$ normal to the surface, is positive for heat transfer to the wall, and $\mathbf{F}'$, being parallel to the surface, is positive when the force tends to accelerate the gas. In the volume integrals of (3.3), ψ_n and $\nabla\psi_n$ are essentially independent of y, so one can write

$$\int Q'\psi_n \,\mathrm{d}v \approx \iint \mathrm{d}S\psi_n \int_0^\infty \frac{\partial q_y'}{\mathrm{d}y}\,\mathrm{d}y = -\iint q_w'\psi_n \,\mathrm{d}S \tag{3.6}$$

$$\int \mathbf{F}' \cdot \nabla\psi_n \,\mathrm{d}v \approx \iint \mathrm{d}S\nabla\psi_n \cdot \int_0^\infty \frac{\partial \tau_y'}{\partial y}\,\mathrm{d}y = -\iint \tau_w' \cdot \nabla\psi_n \,\mathrm{d}S. \tag{3.7}$$

Here, the surface stress is $\tau_w' = -\mu(\partial \mathbf{u}'/\partial y)_w$, where $\mathbf{u}'$ is the velocity fluctuation parallel to the surface, so

$$-\iint \tau_w' \cdot \nabla\psi_n \,\mathrm{d}S = \iint \left(\mu\frac{\partial \mathbf{u}'}{\partial y}\right)_w \cdot \nabla\psi_n \,\mathrm{d}S. \tag{3.8}$$

Only the linear stress will be treated, but both linear and nonlinear contributions to the heat transfer will be accommodated by writing

$$q_w' = \left(k\frac{\partial T'}{\mathrm{d}y}\right)_w + \bar{h}(T_\infty' - T_w'). \tag{3.9}$$

Owing to the thermal inertia of the wall, $T_w' \approx 0$; the temperature fluctuation T_∞' far from the wall is that associated with the acoustic field. The average heat transfer coefficient, $\bar{h}$, will be assumed in a manner described below, to depend on the amplitude of the acoustic field.

Equation (3.3) can now be written

$$\ddot{\eta}_n + \omega_n^2\eta_n = -\frac{\bar{\gamma}}{\rho_o E_n^2}\iint \left(\mu\frac{\partial \mathbf{u}'}{\partial y}\right)_w \cdot \nabla\psi_n \,\mathrm{d}S - \frac{\bar{R}/\bar{C}_v}{p_o E_n^2}\frac{\mathrm{d}}{\mathrm{d}t}\iint \left(k\frac{\partial T'}{\mathrm{d}y}\right)_w \psi_n \,\mathrm{d}S$$
$$- \frac{\bar{R}/\bar{C}_v}{p_o E_n^2}\frac{\mathrm{d}}{\mathrm{d}t}\iint \bar{h}T_\infty'\psi_n \,\mathrm{d}S. \tag{3.10}$$

First, calculation of the linear parts will be outlined. The known solutions for

the velocity and temperature fluctuations in a sinusoidal acoustic field are

$$u' = \hat{u}[1 - e^{-\lambda y}]e^{i\omega t}$$
$$T' = \hat{T}[1 - e^{-(Pr)^{1/2}\lambda y}]e^{i\omega t} \tag{3.11}$$

where $\hat{u}$, $\hat{T}$ are the amplitudes far from the wall, and

$$\lambda = \frac{1}{\delta}(1+i) \quad \delta = \sqrt{(2\bar{\nu}/\omega)}. \tag{3.12}$$

Thus, for purely harmonic oscillations,

$$\left(\mu\frac{\partial u'}{\partial y}\right)_w = \frac{\mu}{\delta}(1+i)\hat{u}\,e^{i\omega t}$$
$$\left(k\frac{\partial T'}{\partial y}\right)_w = \frac{k}{\delta}(Pr)^{1/2}(1+i)\hat{T}\,e^{i\omega t}.$$

These formulas are for steady oscillations. For transient motions, exact results can be obtained, but those are too complicated for the purposes here. Instead, the following approximation is used. Note that for sinusoidal motions, i may be replaced by $\omega^{-1}\partial/\partial t$. This replacement will be made, and $\hat{u}$ and $\hat{T}$ will be taken to stand for the values associated with each mode. For the nth mode one eventually finds that (3.10) may be written

$$\ddot{\eta}_n + \omega_n^2\eta_n = -2\alpha_n^{(\omega)}(\dot{\eta}_n - \omega_n\eta_n) - \frac{\bar{R}/\bar{C}_v}{p_o E_n^2}\left(\frac{\bar{\gamma}-1}{\bar{\gamma}}\right)T_o\frac{d}{dt}\int\int \bar{h}\eta_n\psi_n^2\,dS \tag{3.13}$$

where

$$\alpha_n^{(\omega)} = \frac{(\omega_n\bar{\nu}/2)^{1/2}}{2(1+\kappa)}\frac{1}{E_n^2}\int\int\left[\left(\frac{\nabla\psi_n}{k_n}\right)^2 + \frac{\bar{\gamma}-1}{\sqrt{(Pr)}}\right]\int\int \psi_n^2\,dS. \tag{3.14}$$

It has been assumed that the motion far from the wall is isentropic, so $T'_\infty = (\bar{\gamma}-1)(T_o p'/\bar{\gamma}p_o)$. For a longitudinal mode in a straight cylindrical tube,

$$\int\int\left(\frac{\nabla\gamma_n}{kn}\right)^2 dS = \int\int \psi_n^2\,dS = \pi DL/2$$

and with $\kappa = 0$, (3.14) becomes the familiar result for the decay constant for a standing longitudinal wave:

$$\alpha_n^{(\omega)} = \frac{2}{D}\sqrt{\left(\frac{\omega_n\bar{\nu}}{2}\right)}\left(1 + \frac{\bar{\gamma}-1}{\sqrt{(Pr)}}\right).$$

The treatment of the remaining term in (3.13) rests on appeal to some recent experimental results. Perry and Culick (1974) have reported measurements of the

time- and space-averaged values of the heat transfer coefficient in a T-burner with propellant discs at the ends. Denote this coefficient by $\langle \bar{h} \rangle$. The data could be quite well represented by the expression

$$\frac{\langle \bar{h} \rangle \delta}{k} = 0.044 Re_n^{1/2} \tag{3.15}$$

where

$$Re_n = \frac{|\hat{p}|_m \delta}{\mu \bar{a}}. \tag{3.16}$$

The symbol $|\hat{p}|_m$ represents the maximum amplitude of the pressure fluctuation, namely that measured at the end of the T-burner; this is equal to $p_n|\eta_n|$ for the nth mode.

In the absence of any other information, two assumptions will be made. First, it is reasonable to assume that the local time-averaged heat transfer coefficient is also proportional to the square root of the pressure amplitude, as (3.15) shows for the space-averaged value. Hence, for the nth mode,

$$\bar{h} = K_n |\psi_n \eta_n|^{1/2} \tag{3.17}$$

where K_n is a constant to be determined. The second assumption is that (3.17) is valid for all modes. From the definitions of $\bar{h}$ and $\langle \bar{h} \rangle$,

$$\langle \bar{h} \rangle = \frac{1}{S} \iint \bar{h} \, dS = \frac{1}{L} \int_0^L \bar{h} \, dz \tag{3.18}$$

for a cylinder. It follows from (3.15)–(3.18) that the constant K_n is given as

$$K_n = 0.044 \frac{k \sqrt{(p_n)}}{\sqrt{(\mu \bar{a})}} \left(\frac{\omega_n}{2\bar{\nu}} \right)^{1/4} \left[\frac{1}{L} \int_0^L |\psi_n|^{1/2} \, dz \right]^{-1}.$$

The integral has the value

$$\frac{1}{L} \int_0^L |\psi_n|^{1/2} \, dz = \frac{1}{L} \int_0^L |\cos k_n z|^{1/2} \, dz = 0.765$$

so

$$K_n = 0.0575 \frac{k \sqrt{(p_n)}}{\sqrt{(\mu \bar{a})}} \left(\frac{\omega_n}{2\bar{\nu}} \right)^{1/4}. \tag{3.19}$$

Note that the mode shape $\cos(k_n z)$ is used to obtain (3.19) because the data was taken in a uniform tube. The assumptions introduced above imply that the result is supposed to be valid for a local surface element whatever may be the mode in the chamber.

After the method of averaging has been applied, and various integrals have

been evaluated (see Culick, 1975), equations for A_n and B_n, with only the viscous losses shown are

$$\frac{dA_n}{dt} = -\alpha_n^{(v)}(A_n - B_n) - 0.457H_nA_n(A_n^2 + B_n^2)^{1/4} \tag{3.20}$$

$$\frac{dB_n}{dt} = -\alpha_n^{(v)}(A_n + B_n) - 0.457H_nB_n(A_n^2 + B_n^2)^{1/4}. \tag{3.21}$$

In the special circumstance when these equations are applied to waves in a cylindrical chamber with an inert lateral boundary,

$$J_n = \frac{1.836}{R_c}$$

where R_c is the radius of the chamber; and

$$0.457H_n = \frac{1.143}{R_c}\frac{\bar{\gamma}-1}{Pr\bar{\gamma}^{1/2}}\left[\left(\frac{\bar{\nu}}{10^{-4}}\right)\left(\frac{f_n}{1000}\right)\left(\frac{\bar{a}}{1000}\right)^2\right]^{1/4} \tag{3.22}$$

where the units are: R_c, m; $\bar{\nu}$, m^2/sec; f_n, Hz; and $\bar{a}$, m/sec.

4. An approximation to the influence of transient surface combustion

The source of the energy for unsteady motions in a combustion chamber is the combustion itself. Interactions between combustion and unsteady fluid motions are commonly represented by some sort of frequency response function, which is particularly appropriate for studying the stability of sinusoidal disturbances. The use of a response function is not limited to linear problems, but the problem is much more complicated for nonlinear behavior. Only the simplest representation of the influence of unsteady combustion processes will be covered here. Elementary results for linear response to harmonic pressure variations form the basis. Certain of the features of truly transient behavior will be ignored in the interest of obtaining formulas which are clear and inexpensive to use. Only surface combustion will be discussed, but the same strategy may be used for combustion within the volume.

The influence of surface combustion is contained in $\mathscr{R}$, defined by eqn (3.18) of Part I. It follows from (3.16) and (4.1) of I that the corresponding contribution to the force F_n in (1.6) is

$$F_n^{(c)} = \frac{\bar{\gamma}}{\rho_o E_n^2}\frac{\partial}{\partial t}\iint \mathscr{R}\psi_n \, dS. \tag{4.1}$$

To simplify the discussion, consider only one of the pieces of $\mathscr{R}$; e.g. let $\delta_\perp = 1$, $\delta_\parallel = 0$, so (3.18) of I is

$$\mathscr{R} = \rho_o u_b' + \bar{u}_b\frac{p'}{a_o^2} = (1+\kappa)\left(m_b' + \bar{m}_b\frac{\Delta T'}{T_o}\right). \tag{4.2}$$

It is best here also to avoid the complications associated with a condensed phase: set $\kappa = 0$, so the following results apply to propellants not containing metal.

There exists a class of analyses, discussed by Culick (1968), which produces a formula for $\hat{m}_b/\bar{m}_b$, the fluctuation of mass flux due to a sinusoidal variation of pressure. This is a linear result, $\hat{m}_b/\bar{m}_b$ being proportional to the pressure fluctuation:

$$\frac{\hat{m}_b}{\bar{m}_b} = R_b \frac{\hat{p}}{p_o} = [R_b^{(r)} + iR_b^{(i)}]\frac{\hat{p}}{p_o}. \tag{4.3}$$

The response function, R_b, is a complex function of frequency,

$$R_b = \frac{nAB}{\lambda + \dfrac{A}{\lambda} - (1 + A) + AB}, \tag{4.4}$$

in which A is proportional to the activation energy for the surface reaction, and B depends on both A and the heat released by the surface reaction. Out of the same analyses, one can extract the formula for $\Delta\hat{T}/T_o$; and with these results, (4.2) becomes, for sinusoidal motions,

$$\begin{aligned}\hat{\mathcal{R}} &= \rho_o \bar{u}_b \left[\left(1 + \frac{\bar{T}_s}{T_o}\frac{C}{C_p}\frac{AB}{E}\right)R_b - \left(n\frac{\bar{T}_s}{T_o}\frac{C}{C_p}\frac{AB}{E} + \frac{\gamma - 1}{\gamma}\right)\right]\frac{\hat{p}}{p_o} \\ &= \rho_o \bar{u}_b [\mathcal{R}^{(r)} + i\mathcal{R}^{(i)}]\frac{\hat{p}}{p_o}.\end{aligned} \tag{4.5}$$

Note that $\mathcal{R}^{(r)}$ and $\mathcal{R}^{(i)}$ are dimensionless functions of the frequency and the other parameters; if nonisentropic temperature fluctuations are ignored, $\mathcal{R}_i^{(r)} = R_b^{(r)}(\omega_i)$ and $\mathcal{R}_i^{(i)} = R_b^{(i)}(\omega_i)$.

Now the formula (4.5) is, by construction, for steady sinusoidal variations only. As in the preceding section, the replacement $i \to \omega^{-1}\,\partial/\partial t$ will be made in (4.5), and the result is assumed to apply to all modes. Thus, $\hat{p}/p_o$ stands for $\eta_i\psi_i$, and for an arbitrary pressure field expanded in the form (1.3), $\mathcal{R}$ in (4.1) will hereafter be taken as

$$\mathcal{R} = \rho_o \bar{u}_b \sum_{i=1}^{\infty} \left[\mathcal{R}_i^{(r)} + \frac{1}{\omega_i}\mathcal{R}_i^{(i)}\frac{\partial}{\partial t}\right]\eta_i\psi_i. \tag{4.6}$$

The subscript $(\,)_i$ on $\mathcal{R}_i^{(r)}$ and $\mathcal{R}_i^{(i)}$ means that each function is evaluated at the frequency of the ith mode; these quantities can be calculated from (4.5) and (4.4).

The force (4.1) can now easily be evaluated, and the rule (1.13) gives directly the contributions from surface combustion to $\alpha_n^{(c)}$ and $\theta_n^{(c)}$ to be used in (1.11) and (1.12):

$$\alpha_n^{(c)} = \frac{\gamma \bar{u}_b}{2E_n^2}\mathcal{R}_i^{(r)} \oiint \psi_n^2 \, dS \tag{4.7}$$

$$\theta_n^{(c)} = -\frac{\mathcal{R}_n^{(i)}}{\mathcal{R}_n^{(r)}}\alpha_n^{(c)}. \tag{4.8}$$

The same procedure can be applied to propellants containing metal; only some details are changed to account for $\kappa \neq 0$.

A similar approximation can be used for handling combustion within the volume of a chamber as one finds in liquid rockets, thrust augmentors, and solid rockets exhibiting residual combustion. Although other contributions will in general arise, associated with mass and momentum exchange, the direct contribution of energy release is represented by the terms containing Q and w_v in eqn (2.2) of I. The dynamical behavior of combustion within the volume may, for example, be represented by some sort of response function; the well-known $n-\tau$ model developed by Crocco *et al.* is a special form. In any case, the contributions to the individual harmonics can be approximated as surface combustion was handled above. No results for bulk combustion have been obtained.

5. Application to the stability of longitudinal modes in a rocket motor

It has already been shown that the nonlinear terms simplify considerably for the case of longitudinal modes. This situation will be treated here for one example. Some preliminary results were reported by Levine and Culick (1974). Application to large motors was examined by Culick and Kumar (1974). The discussion here is to demonstrate how the approximate analysis can be used to study practical configurations and to provide a limited comparison with the more exact numerical results reported elsewhere.

For all the calculations reported in this section, the following material and thermodynamic properties are used:

Specific heat of the gas	$C_p = 2021.8 \dfrac{\text{J}}{\text{kgm-°K}}$
Specific heat of the particle material	$C_s = 0.68 C_p$
Thermal diffusivity of the propellant	$\kappa = 10^{-7}\ \text{m}^2/\text{sec}^2$
Prandtl number of the gas	$Pr = 0.8$
Viscosity of the gas	$\mu = 8.834 \times 10^{-4}(T/3485)^{0.66} \dfrac{\text{kgm}}{\text{m-sec}}$
Isentropic exponent of the gas	$\gamma = 1.23$
Linear burning rate of the propellant	$\bar{r} = 0.00812(p_c/500)^{0.3}\ \text{m/sec}$
Density of the propellant	$\rho_c = 4000\ \text{kgm/m}^3$
Density of the condensed material	$\rho_s = 1766\ \text{kgm/m}^3$

Because the nonlinear acoustics terms represented by the series in (1.11) and (1.12) are given explicitly, the first step in the analysis consists in evaluating the contributions to the linear coefficients α_n and θ_n. Four contributions to linear stability are included; arising from the nozzle, the condensed material in the gas phase, the surface combustion processes, and the one-dimensional approximation to inelastic acceleration of flow issuing from the lateral surface ("flow turning"). The formulas for the corresponding values of α_n are

Nozzle

$$\alpha_n = -\bar{a}\left(\frac{J}{L}\right)\left(\frac{2}{\gamma+1}\right)^{(\gamma+1)/2(\gamma-1)} \tag{5.1}$$

Particles

$$\alpha_n = -\frac{1}{2}\left(\frac{\kappa}{1+\kappa}\right)\left[X_1 + (\bar{\gamma}-1)\frac{C}{C_p}X_2\right]_{\omega=\omega_n} \tag{5.2}$$

Flow Turning

$$\alpha_n = -\frac{1}{2}\bar{u}_b\left(\frac{S_b}{V}\right) \tag{5.3}$$

Combustion

$$\alpha_n = \frac{1}{2}\bar{\gamma}\bar{u}_b\left(\frac{S_b}{V}\right)R_b^{(r)}. \tag{5.4}$$

The formula (5.1) is based on quasi-steady behavior; the velocity fluctuations are in-phase with pressure fluctuations at the nozzle entrance. Hence, the response function has no imaginary part and, as shown by eqn (4.10), the value of θ_n for the nozzle is zero. The term representing flow-turning is the last one of (3.17) in I; there is no corresponding E_{ni}, so θ_n is also zero for flow turning. The only non-zero values of θ_n are for the gas/particle interactions and combustion; the first is given by (2.12) and the second by use of (4.8) and (5.4):

Particles

$$\theta_n = \frac{\omega_n}{2}\left(\frac{\kappa}{1+\kappa}\right)\left[\frac{\Omega_d^2}{1+\Omega_d^2} + (\bar{\gamma}-1)\frac{C}{\bar{C}_p}\frac{\Omega_t^2}{1+\Omega_t^2}\right]_{\omega=\omega_n} \tag{5.5}$$

Combustion

$$\theta_n = -\frac{1}{2}\bar{\gamma}\bar{u}_b\left(\frac{S_b}{V}\right)R_b^{(i)}. \tag{5.6}$$

The two examples treated here were discussed in Section 7.4 of Culick and Levine (1974), where the result of the numerical analysis is given. Each is for a motor having a cylindrical bore and length 23.5 in. The mean pressure, port area, and throat area differ and are given below:

	(a)	(b)
Length (in.)	23.5	23.5
Port area (in^2)	3.33	4.73
Throat area (in^2)	0.439	0.562
Pressure (psia)	1568	1412

These are the first and last cases given in Table 7.3 by Culick and Levine (1974). The fundamental frequency is 900 Hz.

For both cases, the particle diameter is assumed to be 2.0μ and the mass fraction is $\kappa = 0.36$. The combustion response is taken to be the representation (7.4) given above, with $A = 6.0$ and $B = 0.56$. Because the pressures are different, so are the flame temperatures in the two cases; for (a), $T_f = 3525°K$ and for (b), $T_f = 3515°K$. The small difference has only minor influence on the results.

With the above values, and the formulas (5.1)–(5.4), waves for case (a) are found to be stable. The values of the decay constants for the first five modes are given in Table 5.1. The numerical calculations produced an unstable wave which, with an initial amplitude of 5% (fundamental mode) eventually reached a limiting amplitude of 4.2%. In view of the successful comparison for the cases treated in Section 2 for attenuation by particle damping, and because the representation of the combustion response is the same in the approximate and numerical analysis, a likely source of the difference in the results is the behavior of the nozzle.

Table 5.1. Values of α_n and θ_n for three cases of unsteady motions in a small motor

	Case (a) (sec^{-1})	Case (aa) (sec^{-1})	Case (b) (sec^{-1})
α_1	−18.5	8.0	−9.1
α_2	−369.3	−342.8	−334.8
α_3	−610.1	−583.6	−566.5
α_4	−915.9	−889.4	−871.4
α_5	−1289.2	−1262.7	−1244.0
θ_1	12.9	12.9	64.0
θ_2	46.8	46.8	34.9
θ_3	−29.3	−29.3	−35.6
θ_4	−131.0	−131.0	−135.0
θ_5	−280.0	−280.0	−283.0

In the numerical analysis, the calculations for the entire two-phase flow were carried out to the nozzle throat. The influence of the nozzle is buried in the results and its contribution to attenuation cannot be determined. For the approximate analysis, the influence of the nozzle is represented as a surface admittance function evaluated at the nozzle entrance. The result (5.1) is strictly valid for quasi-steady behavior of a gas only; it has been extended to the case of two-phase flow by using the value of $\bar{\gamma}$ for the mixture. The point is that there is reason to expect that the contribution of the nozzle is different in the two analyses.

As a means of comparing the analyses, the value of the attenuation constant associated with the nozzle is chosen to obtain the same limiting amplitude as found in the numerical analysis. This procedure rests on the observation that the values of the limiting amplitudes are quite sensitive to the values of the linear coefficients α_n, θ_n.

Not a very large change is required. Equation (5.1) gives $\alpha_n = -153.25\ sec^{-1}$. If this is changed to $-126.75\ sec^{-1}$, then $\alpha_1 = 8.00$ and the limiting amplitude is

about 4.2%. The values of the α_n and θ_n for five modes are given in Table 5.1, for the case denoted (aa). Figure 5.1 shows the amplitudes of the five harmonics considered; the functions A_n and B_n are shown in Figs. 5.2 and 5.3. The waveform at limiting amplitude shows no obvious evidence of distortion from the fundamental mode.

The attenuation by the nozzle is assumed to vary linearly with the ratio J of throat area to port area, having the value $-126.75\,\text{sec}^{-1}$ when J has the value (0.132) for case (a). Then with the other required data given above, the

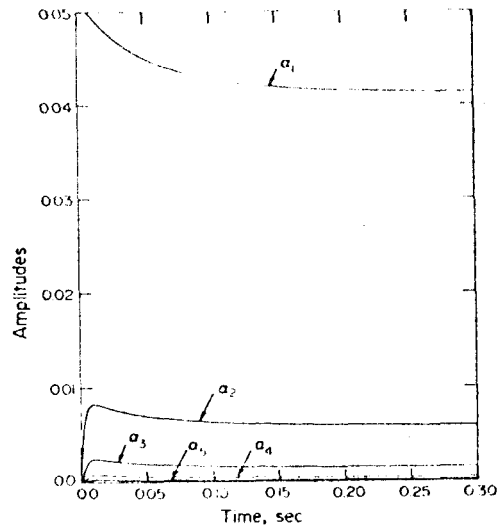

Fig. 5.1. Amplitudes for unstable oscillations in a motor, case (aa) of Table 5.1.

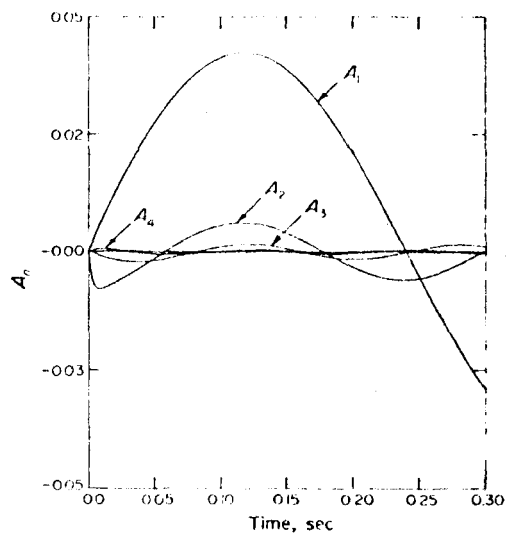

Fig. 5.2. The functions $A_n(t)$ for case (aa) of Table 5.1.

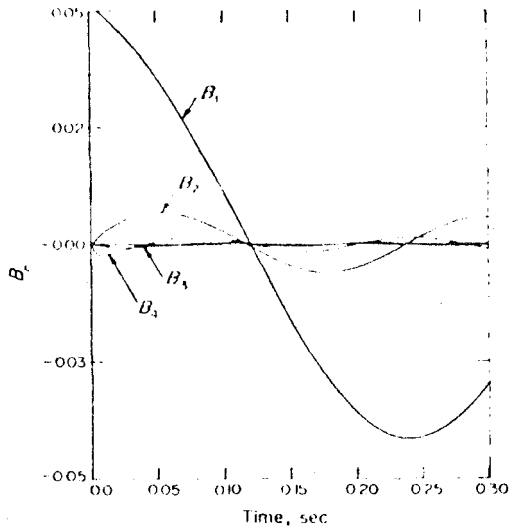

Fig. 5.3. The functions $B_n(t)$ for case (aa) of Table 5.1.

approximate analysis applied to case (b) produces the results shown in the last column of Table 5.1. The initial disturbance is stable, the decay constant for the first harmonic being $\alpha_1 = -9.12\,\text{sec}^{-1}$. After twenty cycles (0.02222 sec) the amplitude is roughly 3.5% according to the approximate analysis. The numerical analysis gave an amplitude of 3.02% after twenty cycles. It appeared that the wave may have stabilized at a limiting amplitude, but the calculation was not carried further. In view of the slow decay found with the approximate analysis, it may be that the conclusion based on the numerical analysis, for only 20 cycles, is incorrect, based on incomplete results. If a true limit was indeed reached, then of course the approximate analysis gives the wrong result. A limit of 3% would be reached only if α_1 is positive, having a value less than 8.00.

That nonlinear influences are in fact active, even at such relatively small amplitudes, is easily established. Consider a wave having a decay constant equal to $-9.12\,\text{sec}^{-1}$ and a frequency of 900 Hz. According to linear behavior, the amplitude would be 4.08% after 20 cycles if the initial amplitude is 5%. The more rapid decay shown by the nonlinear analysis is evidently due to the transfer of energy, through the nonlinear processes, from the fundamental oscillation to higher harmonics which are then attenuated much more rapidly. Nonlinear particle damping was included in the approximate analysis but, as one should expect for the small amplitudes arising in these examples, its influence is negligibly small.

An example of longitudinal modes in a T-burner has been treated elsewhere by Culick (1976).

Acknowledgments--This work was supported partly by Hercules, Inc., Magna, Utah; by the Aerojet Solid Propulsion Co., Sacramento, California; and by the National Aeronautics and Space Administration under the Jet Propulsion Laboratory Contract NAS 7-100.

References

Culick, F. E. C. (1968) A review of calculations for unsteady burning of a solid propellant, *AIAA J.* **6**(12), 2241–2255.

Culick, F. E. C. (1975) *Nonlinear behavior of acoustic waves in combustion chambers.* Daniel and Florence Guggenheim Jet Propulsion Center, California Institute of Technology, Pasadena, California.

Culick, F. E. C. (1976) Nonlinear behavior of acoustic waves in combustion chambers—I, *Acta Astronautica* **3**, 9/10, 715–734.

Culick, F. E. C. and Kumar, R. N. (1974) *Combustion instability in large solid rocket motors*, 10th JANNAF Combustion Meeting, Newport, Rhode Island.

Culick, F. E. C. and Levine, J. N. (1974) *Comparison of approximate and numerical analyses of nonlinear combustion instability*, AIAA 12th Aerospace Sciences Meeting, Washington, D.C. AIAA Paper No. 74-201.

Levine, J. N. and Culick, F. E. C. (1972) *Numerical analysis of nonlinear longitudinal combustion instability in metallized propellant solid rocket motors.* Ultrasystems, Inc., Irvine, Calif., Technical Report AFRPL-TR-72-88.

Levine, J. N. and Culick, F. E. C. (1974) *Nonlinear analysis of solid rocket combustion instability.* Ultrasystems, Inc., Irvine, Calif., Technical Report AFRPL-74-45.

Perry, E. H. and Culick, F. E. C. (1974) Measurement of wall heat transfer in the presence of large-amplitude combustion-driven oscillations, *Comb. Sci. Technol.* **9**, 49.

Temkin, S. and Dobbins, R. A. (1966) Attenuation and dispersion of sound by particulate-relaxation processes, *J. Acoust. Soc. Am.* **40**(2), 317–324.

Appendix A

Nomenclature

Some symbols defined in the text and used but briefly are not included here. A complete list of symbols appears in Part I.

$\bar{a}^2$ $\bar{\gamma}p_m/\rho_m$ average speed of sound for the mixture

A_n eqn (1.7)

B_n eqn (1.7)

C specific heat of particulate material

C_p, C_v specific heats of gases

$\bar{C}_p, \bar{C}_v$ specific heats of gas/particle mixture

E_m eqn (1.10)

k complex wavenumber, $k = (\omega - i\alpha)/a_m$

k_l wavenumber for longitudinal or axial modes

k_n wavenumber for three-dimensional normal modes

L length of chamber

m_b mass flux of gases inward at the burning surface

m_b^p mass flux of particulate material inward at the burning surface

M_b Mach number of the gases at the edge of the combustion zone, $\bar{u}_b/a_m$

p pressure

p_m average pressure

q perimeter of the chamber cross section

R mass-averaged gas constant

$\bar{R}$ mass-averaged gas constant for the gas/particle mixture

$\mathcal{R}$ eqn (4.2)

S_b total area of burning surface

S_c cross section area

T temperature of gases in the chamber

T_p temperature of particulate material

T_s temperature of gases at the edge of the combustion zone

$\mathbf{u}$ velocity of the gases

$\mathbf{u}_p$ velocity of the particulate material

u_b speed of gases entering at the burning surface

V volume

α attenuation or growth constant

γ ratio of specific heats for the gases, C_p/C_v

$\bar{\gamma}$ ratio of specific heats for the gas/particle mixture, $\bar{C}_p/\bar{C}_v$

κ mass fraction of particulate material, ρ_p/ρ_g

η_n eqn (1.7)

ρ density of the gas/particle mixture, $\rho = \rho_g + \rho_p$

ρ_g density of the gases

ρ_{gm} average value of ρ_g

ρ_p density of the particulate matter (mass per unit volume of chamber)

ρ_{pm} average value of ρ_p

ρ_m average density of the gas/particle mixture

σ diameter of particles

τ_d $\tau_d = \rho s\sigma^2/18\mu$

τ_t $\tau_t = (3CPr/2C_p)\tau_d$

ψ_l normal mode shapes for one-dimensional problems

ψ_n normal mode shapes for three-dimensional problems

ω_l angular frequency for one-dimensional normal modes

ω_n angular frequency for three-dimensional normal modes

Ω_l, Ω_n $\Omega_l = \omega\tau_d; \Omega_n = \omega\tau_t$